DOI: 10.61458/jepm.2024.213
UDC: 536.5:537.226:519.6

Journal of
Engineering & Processing Management

ORIGINAL SCIENTIFIC PAPER

Computational fluid dynamics implementation and optimization of electrohydrodynamics' two-phase leaky dielectric model

Stefan A. Bošković [1] | Aleksandar Karač [2] | Slobodan B. Vrhovac [3] | Aleksandar Belić [3] | Branko Bugarski [4]

[1]Innovation Center of the Faculty of Technology and Metallurgy in Belgrade Ltd., Karnegijeva 4, 11120 Belgrade, Serbia

[2]Polytechnic Faculty, University of Zenica, Fakultetska 1, 72000 Zenica, Bosnia and Herzegovina

[3]Institute of Physics Belgrade, University of Belgrade, Pregrevica 118, 11080 Belgrade, Serbia

[4]Faculty of Technology and Metallurgy, University of Belgrade, Karnegijeva 4, 11120 Belgrade, Serbia

Correspondence
Stefan A. Bošković
Email: sboskovic@tmf.bg.ac.rs

Abstract

The leaky dielectric model from electrohydrodynamics (EHD) was incorporated into the computational fluid dynamics (CFD) software called OpenFOAM®. Based on the used literature, it can be said that this implementation of the mentioned model is the most complete. Three sets of two-phase simulations were done. The first set was one-dimensional. In the second set, a stationary drop surrounded by another fluid deformed under the influence of an electric field. The deformations were both positive and negative. These two sets were used in order to optimize the implementation. Different expressions were tested. A new way for calculating the electrostrictive force when there are two fluids is presented. It resolves the previously encountered issue concerning drop deformations. Recommendations for expressions used in OpenFOAM® for all three electric forces are given. Finally, a settling drop within an electric field was simulated. The final set of simulations more obviously shows the usability of this implementation in practice. Conclusions that are presented in this paper can be transferred to other EHD models and their implementations.

Keywords: EHD, CFD, OpenFOAM®, two-phase, electrostrictive force, drop settling

1. INTRODUCTION

Electrohydrodynamics (EHD) is the part of physics that is dedicated to motion of a liquid in the presence of an electric field (Bošković, Karač, Vrhovac, Belić, & Bugarski 2022a). EHD has existed for perhaps more than a century, and the literature about it ranges from books to scientific articles (Bošković, Karač, Vrhovac, Belić, & Bugarski 2022b). The interest in EHD that exists today is not surprising because of the number of processes for which it can be applied. Some of them are the electrospraying process He and Jokerst (2020), the electrospinning process (Vaseashta & Bölgen 2022), and the electrocoalescence (Leary, Yeganeh, & Maldarelli 2020), which have different applications (Bošković & Bugarski 2018).

Our groups already used and analyzed a process in which an electric field is used, namely the electrostatic extrusion (Bugarski et al. 1994; Bugarski, Smith, Wu, & Goosen 1993; Manojlovic, Djonlagic, Obradovic, Nedovic, & Bugarski 2006; Poncelet, Babak, Neufeld, Goosen, & Burgarski 1999; Poncelet et al. 1994). We also investigated EHD and used computational fluid dynamics (CFD) for EHD (Bošković et al. 2022a; 2022b). Recently (Bošković & Bugarski 2024), we were the first to derive an electromagnetofluid dynamics (EMFD) model usable for CFD, and we implemented it in a CFD software, and verified it with very complex cases. Thus, investigation of EHD could be viewed as a thing of the past. However, investigation of some issues that have remained unresolved within EHD can still be helpful. Hence, we decided to address them.

There are certain implementations of EHD models, though it can be said that their number is somewhat limited (Bošković et al. 2022a). Similarly, some improvements regarding both EHD and the implementation process of EHD models can be made at this moment that would allow their wider practical usage. Previously, our team implemented a simple EHD model that is called the perfect dielectric model. In this work, an implementa-

tion of a more complex leaky dielectric model (Lima 2017; Munoz 2014) is presented, building on top of our previous conclusions and optimizations. Leaky dielectrics are slightly conducting mediums and the leaky dielectric model has been considered for some time in EHD (Lima 2017). This model can be seen as a final step before starting with a more complex model, but because of its applicability and its lower number of equations (which can be equated to a higher calculation speed), usage of more complex models might be unnecessary in some situations.

Different simulations were done in order to optimize the implementation and to show its applicability. The first set of simulations is one-dimensional and we analyzed it qualitatively. In the second set, a drop deformation is caused by an electric field. This is a standard and frequently the most complex set that is used in EHD for new models (Bošković et al. 2022b; López-Herrera, Popinet, & Herrada 2011). The third set is a set that is arguably rarely investigated so new results can be important for future comparisons. This could be caused by the fact that the analytical equation is much newer (Xu & Homsy 2006). It is a set in which a drop is settling in an electric field.

The leaky dielectric model was incorporated into the CFD software OpenFOAM® (version 10). The solver present therein called interFoam was expanded. The Finite Volume Method (FVM) (Maliska 2023) and the Volume of Fluid (VoF) Method (Ionescu 2018) are used in the starting solver. Thus, they were used in our solver, too.

The paper is presented in the following way: first the model with expressions is presented, followed by the results obtained while using it.

2. MATHEMATICAL MODEL

The expansion of the interFoam solver, in order to include electric field influence, started by introducing new terms for electric forces to the Navier-Stokes equation (Bošković et al. 2022a; 2022b):

$$\frac{\partial(\rho \boldsymbol{U})}{\partial t}+\nabla\cdot(\rho \boldsymbol{U}\boldsymbol{U})-\nabla\cdot(\mu\nabla \boldsymbol{U})=\rho \boldsymbol{g}-\nabla p+\boldsymbol{F}_{st}+\boldsymbol{F}_{C}+\boldsymbol{F}_{oel} \tag{1}$$

where ρ is the mass density, **U** is the velocity, t represents the time, μ is the dynamic viscosity, **g** represents the gravitational acceleration, p represents the pressure, **F** is the force, while subscripts *st*, *C*, and *oel* denote surface tension, Coulombic, and other electric, respectively. As previously done Bošković and Bugarski (2024); Bošković et al. (2022a), $\mathbf{F_C}$ and $\mathbf{F_{oel}}$ were calculated just before **U** and p within the solver, while underlying expressions in the software were not modified. Thus, details about calculation of $\mathbf{F_{st}}$ can be found in the existing literature (Huh & Wirz 2022). $\mathbf{F_{oel}}$ is given by:

$$\boldsymbol{F}_{oel}=\boldsymbol{F}_{diel}+\boldsymbol{F}_{els} \tag{2}$$

where subscripts *diel* and *els* denote dielectric and electrostrictive, respectively.

Equations for Coulombic and other electric forces are derived in the EHD literature from Maxwell stress tensor ($\mathbf{T_e}$) (Bošković et al. 2022b; López-Herrera et al. 2011; Reddy & Esmaeeli 2009):

$$\boldsymbol{T}_{e}=\varepsilon \boldsymbol{E}^{2}-\frac{1}{2}\varepsilon|\boldsymbol{E}|^{2}\boldsymbol{I}+\frac{1}{2}\rho\left(\frac{\partial\varepsilon}{\partial\rho}\right)_{T}|\boldsymbol{E}|^{2}\boldsymbol{I} \tag{3}$$

where ε represents the electric permittivity, **E** is the electric field strength, **I** is the identity tensor, and T represents the temperature. The divergence operator is applied to $\mathbf{T_e}$ for obtaining the aforementioned equations (Bošković et al. 2022b).

2.1. Coulombic force calculation

Various expressions for the Coulombic force were tested.

The first expression is the expression in which the software applies the divergence operator to the appropriate part of $\mathbf{T_e}$ (López-Herrera et al. 2011):

$$\boldsymbol{F}_{C}=\nabla\cdot\left(\varepsilon \boldsymbol{E}^{2}\right) \tag{4}$$

The next expression is the expression that can be derived from Eq. (4) (Lastow & Balachandran 2006; Reddy & Esmaeeli 2009):

$$\boldsymbol{F}_{C}=\rho_{e}\boldsymbol{E} \tag{5}$$

where ρ_e is the electric charge density.

The third expression is the expression that uses cell surface values:

$$\boldsymbol{F}_{C}=\mathrm{R}\left\{-\rho_{e,f}\left[\boldsymbol{n}_{f}\cdot(\nabla\phi)_{f}\right]\left|\boldsymbol{S}_{f}\right|\right\} \tag{6}$$

where R represents the reconstruction function, **n** is the unit normal vector, ϕ is the electric potential, and **S** represents the surface area vector, while the subscript f denotes the cell face.

The last analyzed expression was the following:

$$\boldsymbol{F}_{C}=\frac{1}{\varepsilon}\mathrm{R}\left\{-\rho_{e,f}\varepsilon_{f}\left[\boldsymbol{n}_{f}\cdot(\nabla\phi)_{f}\right]\left|\boldsymbol{S}_{f}\right|\right\} \tag{7}$$

2.2. Dielectric force calculation

Usage of two expressions for the dielectric force was investigated. The first one is the following (Bošković et al. 2022a; 2022b):

$$\boldsymbol{F}_{diel} = \mathrm{R}\left\{-\frac{1}{2}\left(|\boldsymbol{E}|^2\right)_f \left[\boldsymbol{n}_f \cdot (\nabla\varepsilon)_f\right] |\boldsymbol{S}_f|\right\} \tag{8}$$

while the second one is (Bošković et al. 2022a; 2022b):

$$\boldsymbol{F}_{diel} = \mathrm{R}\left\{-\frac{1}{2}\left|\boldsymbol{n}_f \cdot (\nabla\phi)_f\right|^2 \left[\boldsymbol{n}_f \cdot (\nabla\varepsilon)_f\right] |\boldsymbol{S}_f|\right\} \tag{9}$$

2.3. Electrostrictive force calculation

A new way of calculating the electrostrictive force is given here. The electrostrictive force is calculated using the expression similar to the one already used for polar fluids in the literature (Bošković et al. 2022a):

$$\boldsymbol{F}_{els} = \nabla\left(\frac{1}{2} f_{els}\varepsilon |\boldsymbol{E}|^2\right) \tag{10}$$

where f represents a function. Eq. (10) was implemented in OpenFOAM® in the following way (Bošković et al. 2022a):

$$\boldsymbol{F}_{els} = \mathrm{R}\left\{\left\{\boldsymbol{n}_f \cdot \left[\nabla\left(\frac{1}{2} f_{els}\varepsilon |\boldsymbol{E}|^2\right)\right]_f\right\} |\boldsymbol{S}_f|\right\} \tag{11}$$

The electrostrictive function is:

$$f_{els} = \alpha_1 f_{els,1} + \alpha_2 f_{els,2} \tag{12}$$

where α is the volume fraction, while the subscript j ($j = 1, 2$) denotes the fluid j.

For a nonpolar fluid, $f_{els,j}$ is equal to:

$$f_{els,j} = \frac{1}{3}(\varepsilon + 2\varepsilon_0)\left(\frac{1}{\varepsilon_0} - \frac{1}{\varepsilon}\right) \tag{13}$$

where the subscript 0 denotes the vacuum. Thus, if both fluids are nonpolar, Eq. (10) reduces to the usual equation for that case (Bošković et al. 2022a).

On the other hand, for a polar fluid, $f_{els,j}$ becomes the empirical factor (Bošković et al. 2022a). For example, if one of the fluids is water, a value of 1.5 can be used for $f_{els,j}$ (Kunti, Bhattacharya, & Chakraborty 2017; Shneider & Pekker 2013). Therefore, if both fluids are polar, Eq. (10) becomes the expression that can be found in (Bošković et al. 2022a) for the same case. Other types of expressions for polar fluids can be introduced analogously.

Obviously, this way of calculating the electrostrictive force is different from the previously available one in (Bošković et al. 2022a) when one of the fluids is polar, while the other one is nonpolar. A discontinuity in the calculation of $\mathbf{F}_{\mathbf{els}}$ is not present here, while it can be found in (Bošković et al. 2022a).

2.4. Electric charge density calculation

The electric charge density was calculated either from (Huh & Wirz 2022; Thirumalaisamy, Natarajan, & Dalal 2018):

$$\rho_e = \nabla \cdot (\varepsilon \boldsymbol{E}) \tag{14}$$

or from (Dastourani, Jahannama, & Eslami-Majd 2018; Lima & d'Ávila 2014):

$$\rho_e = -\nabla \cdot (\varepsilon \nabla\phi) \tag{15}$$

in order to analyze whether one of these two expressions is better for usage within the software.

2.5. Other calculations

The electric field strength was equal to (Bošković et al. 2022a; Lastow & Balachandran 2006):

$$\boldsymbol{E} = -\nabla\phi \tag{16}$$

The curl of the electric field strength is (Bošković et al. 2022b; López-Herrera et al. 2011):

$$\nabla \times \boldsymbol{E} = \boldsymbol{0} \tag{17}$$

As discussed previously in (Bošković et al. 2022b), Eq. (17) cannot be directly included in the calculation, but the value of $\nabla\times\mathbf{E}$ was calculated to check the quality of the calculation.

The electric potential was calculated from (Munoz 2014; Supeene, Koch, & Bhattacharjee 2008):

$$\nabla \cdot (\sigma \nabla\phi) = 0 \tag{18}$$

where σ is the electric conductivity.

The electric permittivity and the electric conductivity are given by usual expressions for the VoF method (Dastourani et al. 2018; Lima 2017):

$$\varepsilon = \alpha_1\varepsilon_1 + \alpha_2\varepsilon_2 \tag{19}$$

$$\sigma = \alpha_1\sigma_1 + \alpha_2\sigma_2 \tag{20}$$

The reconstruction function that was used in some of the previous expressions is a function that is already

present in OpenFOAM®. It is used for reconstructing a cell center value from cell face values and is equal to (Bošković et al. 2022b):

$$\mathrm{R}(z_f) = \left(\sum_f \boldsymbol{S}_f \frac{\boldsymbol{S}_f}{|\boldsymbol{S}_f|} \right)^{-1} \cdot \left(\sum_f z_f \frac{\boldsymbol{S}_f}{|\boldsymbol{S}_f|} \right) \tag{21}$$

where z is a variable.

Time step sizes were calculated based on the values of the Courant number, the interface Courant number, the electric Courant number, and the interface electric Courant number as described earlier (Bošković et al. 2022b). The electric Courant number is given by (Bošković et al. 2022b):

$$Co_e = \frac{|\boldsymbol{E}| \sqrt{\varepsilon/\rho}}{(\delta x)/(\delta t)} \tag{22}$$

where Co is the Courant number and x is an axis, while the subscript e denotes electric.

3. RESULTS AND DISCUSSION

Here, two fluids were named Fluid 1 and Fluid 2. These fluids were needed to conduct the simulations presented here because the systems consisted of two fluids. Properties of these fluids, along with differences between them, are given in the following text. Unless stated otherwise, both fluids were nonpolar and Eq. (8) was used for $\mathbf{F}_{\mathbf{diel}}$.

Volume fractions were calculated using the Interface Compression scheme. Target maximum values for the electric Courant number and the interface electric Courant number were 0.2. The same value was used for the Courant number and the interface Courant number, unless stated otherwise. When our new solver was used, the starting value for the first time step was equal to the time interval used for outputting results. Thus, it can be checked whether the electric Courant numbers aid in determining the appropriate time step length. Meshes were static because of the previously reported errors with dynamic meshes (Bošković et al. 2022b). Mesh densities were constant.

3.1. One-dimensional analysis

The one-dimensional geometry is a 0.1 m long domain, with Fluid 1 filling the first part of the domain and Fluid 2 filling the other part. The domain is divided into 100 cells of the same size. Geometry borders were walls. The electric potential was 0 on the first wall, while it was 150 V on the second wall.

Fluid 1 and Fluid 2 had the same mass densities and the same kinematic viscosities equal to 1200 kg m^{-3} and 10^{-3} m^2 s^{-1}, respectively. The interfacial tension was 0.1 N m^{-1}, while the gravitational acceleration was 0.

The electric permittivity of Fluid 1 and Fluid 2 was 1.2×10^{-10} and 6×10^{-11} F m^{-1}, respectively. The electric conductivity of Fluid 1 and Fluid 2 was 2.5×10^{-12} and 10^{-12} S m^{-1}, respectively. These values were chosen arbitrarily because there are no restrictions for their values in the analytical equations used in the following comparisons. It can be seen in the literature that the absolute values of the electric permittivity and the electric conductivity are sometimes even not stated, as in Lima and d'Ávila (2014).

The target maximum value for all Courant numbers was 0.2. The results were output every 1 s, while 10 s were simulated.

An analytical equation that would account for all the present electric forces (i.e. the Coulombic, the dielectric, and the electrostrictive force) was not found. Therefore, this is a qualitative analysis.

Figure 1 presents the results obtained when Eq. (6) was used for $\mathbf{F}_{\mathbf{C}}$, while either Eq. (14) or Eq. (15) was used for the electric charge density. Since there is one noticeable local maximum with Eq. (15), while there are three local maxima around the center with Eq. (14), usage of Eq. (14) was disregarded.

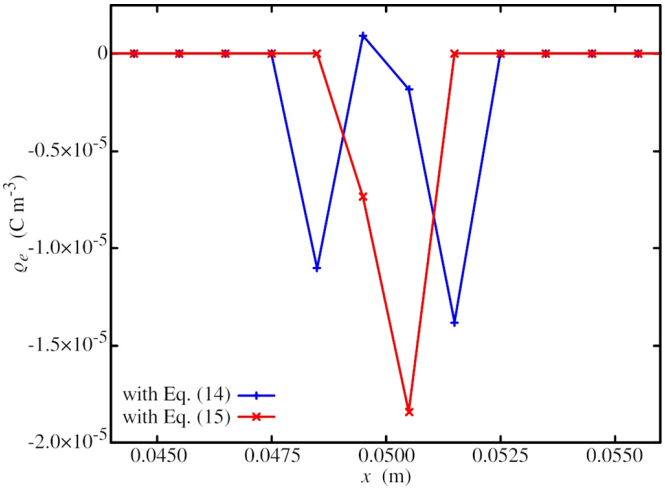

Figure 1. The electric charge density near the center of the geometry when it was calculated using (a) Eq. (14), (b) Eq. (15).

Figure 2 illustrates the obtained velocity magnitudes when the Coulombic force was calculated using different expressions. Since the significantly lower maximum value of $|\mathbf{U}|$ was obtained with Eq. (6) compared to other cases, usage of Eqs. (4), (5), and (7) was disregarded. Eq. (6) is the only expression in which the cell face values are

used and the reconstruction is the final step in the calculation. This result was expected because such expressions were recommended as the best ones for $\mathbf{F}_{\mathbf{diel}}$ and $\mathbf{F}_{\mathbf{els}}$ in (Bošković et al. 2022a; 2022b).

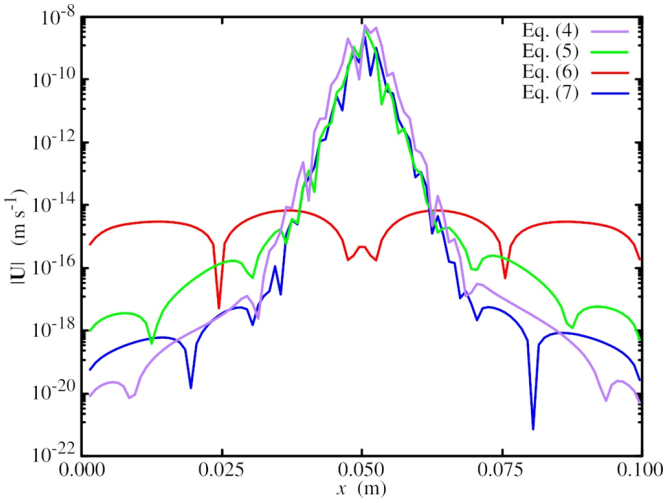

Figure 2. The velocity magnitude when the Coulombic force was calculated using (a) Eq. (4), (b) Eq. (5), (c) Eq. (6), (d) Eq. (7).

3.2. Drop analysis

The geometry used for these simulations is presented in Figure 3. Fluid 1 was the drop fluid, while Fluid 2 was the surrounding fluid. The starting drop diameter was 0.01 m. The bottom border was a symmetry axis. The left and the right border were walls. The electric potential was 0 on the right wall, while its value on the left wall depended on the case. Both fluids could exit through the top border, while Fluid 2 could also enter through it, so the geometry was open, unless stated otherwise. The gradient of the electric potential was 0 on the top border.

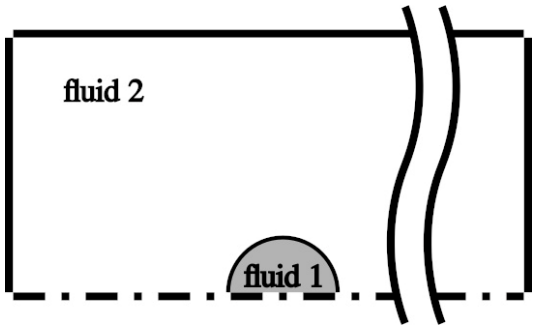

Figure 3. The geometry used for drop simulations.

The drop deformation can be calculated from the following expression (Bošković & Bugarski 2024; Singh, Bahga, & Gupta 2019):

$$D_d = \frac{l_{d,p} - l_{d,n}}{l_{d,p} + l_{d,n}} \tag{23}$$

where D represents the deformation and l represents the length, while subscripts d, p, and n denote drop, direction parallel to $\mathbf{E}$, and direction normal to $\mathbf{E}$, respectively.

The magnitude of the electric field that is macroscopically uniform was calculated from the following expression (Bošković & Bugarski 2024; Lima & d'Ávila 2014):

$$|\boldsymbol{E}_{mu}| = \left| \frac{\phi_l - \phi_r}{l_w} \right| \tag{24}$$

where subscripts mu, l, r, and w denote macroscopically uniform, left, right, and between walls, respectively.

The following ratios are useful for simplifying equations (Behera, Mandal, & Chakraborty 2019; López-Herrera et al. 2011):

$$R_\sigma = \sigma_1/\sigma_2 \tag{25}$$

$$R_\varepsilon = \varepsilon_1/\varepsilon_2 \tag{26}$$

$$R_\mu = \mu_1/\mu_2 \tag{27}$$

where R is a ratio of the property in the subscript of Fluid 1 and Fluid 2.

3.3. Stationary drop

In these cases, deformation of a stationary drop surrounded by another fluid is caused by an electric field. The drop center was at the center of the lower border. $\mathbf{F}_{\mathbf{diel}}$ was calculated from Eq. (8), unless stated otherwise.

Two analytical equations can be found for calculating the deformation (Lima 2017). The first one is the equation that has only a first order approximation (Bošković & Bugarski 2024; Lima 2017):

$$D_d = \varphi_{I,I} Ca_e \tag{28}$$

while the second one is the equation that also has a second order correction (Lima 2017):

$$D_d = \varphi_{I,I} Ca_e + \varphi_{I,II} Ca_e^2 \tag{29}$$

where Ca is the capillary number and φ is a function. The electric capillary number is calculated from (Lima 2017):

$$Ca_e = \frac{r_d|_{t=0}\, \varepsilon_2 |\boldsymbol{E}_{mu}|^2}{\gamma} \tag{30}$$

while the functions from Eqs. (28) and (29) are equal to (Lima 2017):

$$\varphi_{I,I} = \frac{9}{16}\frac{\varphi_{II,I}}{(2+R_\sigma)^2} \tag{31}$$

$$\varphi_{I,II} = \frac{\varphi_{I,I}}{(2+R_\sigma)^2}\left\{\left[\frac{9}{5}\left(\frac{R_\sigma-1}{R_\sigma+2}\right)-\frac{1}{16}\right]\varphi_{II,I} + (R_\sigma-R_\varepsilon)\,\varphi_{II,II}\right\} \tag{32}$$

$$\varphi_{II,I} = 1+R_\sigma^2-2R_\varepsilon+\frac{3}{5}(R_\sigma-R_\varepsilon)\frac{2+3R_\mu}{1+R_\mu} \tag{33}$$

$$\varphi_{II,II} = \frac{23}{20}-\frac{139}{210}\left(\frac{1-R_\mu}{1+R_\mu}\right)-\frac{27}{700}\left(\frac{1-R_\mu}{1+R_\mu}\right)^2 \tag{34}$$

The same values as in one-dimensional study were used for the interfacial tension, the gravitational acceleration, and both mass densities, kinematic viscosities, and electric permittivities, as well as both electric conductivities when drop deformations were positive. When drop deformations were negative, Fluid 1 and Fluid 2 had the electric conductivity equal to 10^{-12} and 2.5×10^{-12} S m^{-1}.

The drop deformations were calculated using the OpenFOAM® built-in post processing utility. It was checked whether the penultimate value of the drop deformation differed by less than 0.1% from the last value. The simulation time was 10 s, unless stated otherwise.

3.3.1. *Geometry and mesh analysis*

Geometries that had different widths and heights were analyzed when D_d calculated from Eq. (28) was 0.12 and the mesh density was 24 cells per $d_d|_{t=0}$, where d is the diameter. For heights and widths that are 3, 4, and 5 times the starting drop radius and diameter, the obtained drop deformation was too unsteady, 0.1256, and 0.1245, respectively. Since the difference between the two last values is less than 1.000%, the geometry that was $4d_d|_{t=0}$ wide and $4r_d|_{t=0}$ high could be used, but it was decided to use the geometry $5d_d|_{t=0}$ wide and $5r_d|_{t=0}$ high because such a geometry was used previously in Bošković and Bugarski (2024) and because the computational heaviness of the calculations was not too great.

Influence of the mesh density was also analyzed. D_d calculated from Eq. (28) was 0.08 for this analysis. The mesh density was varied to be 24, 40, 50, 52, 54, and 70 times greater than $d_d|_{t=0}$. The obtained D_d was 0.1245, 0.1303, 0.1055, 0.1125, 0.1076, and 0.1085, respectively. Since the difference between the result obtained when mesh density was $54d_d|_{t=0}$ and when it was $70d_d|_{t=0}$ was less than 1.000%, the mesh density was set to $54d_d|_{t=0}$.

3.3.2. *Dielectric force expression*

Both expressions for the dielectric force were also tested when D_d calculated from Eq. (28) was 0.08. Obtained D_d was equal to 0.1076 when Eq. (8) was used. On the other hand, the drop did not settle when Eq. (9) was used. Furthermore, the last value of D_d was much greater and equal to 0.1548. Hence, usage of Eq. (9) was disregarded. Although both expressions are correct and almost the same, special care needs to be taken in the implementation process, since unstable behavior was encountered with one of the expressions.

This recommendation differs from the one in (Bošković et al. 2022a), mainly due to the fact that the comparison of Eqs. (8) and (9) in Bošković et al. (2022a) was done on a case that is not suitable for OpenFOAM® numerics. Bošković et al. (2022a) state that Eq. (17) was not satisfied inside the geometry. In our present study, very high values of the curl of the electric field strength were noticed only in the cells that are next to the walls, like in Figure 4(a) of Bošković et al. (2022b).

3.3.3. *Electrostrictive force influence*

We started inclusion of more appropriate expressions for polar fluids in two-phase models in Bošković et al. (2022a). We showed that our way of including the electrostrictive force when both fluids were either nonpolar or polar did not affect the drop deformation, even when the polar fluids were different and had different polarities. Thus, it can be said that it would be more logical if the effect on the drop deformation did not exist if one fluid is polar, while the other one is nonpolar. Additionally, this would be in accordance with (Taylor 2011; Torchigin & Torchigin 2013). But this did not happen in Bošković et al. (2022a). Hence, we are proposing a new way of calculating the electrostrictive force to fix this issue.

Here, D_d calculated from Eq. (28) was 0.08. The obtained results for different fluid polarities are presented in Table 1. D_d differed between these cases by less than 1.000%. The small difference could have been caused by numerical errors, possibly spurious currents (Lebaigue 2010), especially since the geometry is not closed. Since the values of the obtained D_d are close, the influence of the fluid polarity and the electrostrictive force can be included in EHD models in the way presented here.

Figure 4 presents the calculated pressure in the geometry for different fluid polarities. Significant differences of pressure are observable. This is in accordance with (Bošković et al. 2022a; Taylor 2011). Hence, it can be concluded that a significant error in the calculated pressure emerges if the electrostrictive force is neglected. Following this result and this work, the pressure modeling in two-phase EHD could finally be improved.

Table 1. Obtained D_d for fluids with different polarities.

Case name	Fluid 1		Fluid 2		D_d (/)
	Polarity	$f_{els,1}$ (/)	Polarity	$f_{els,2}$ (/)	
NpNp	nonpolar	Eq. (13)	nonpolar	Eq. (13)	0.1076
NpP	nonpolar	Eq. (13)	polar	1.5	0.1077
PNp	polar	1.5	nonpolar	Eq. (13)	0.1076
PP	polar	1.5	polar	0.1	0.1080

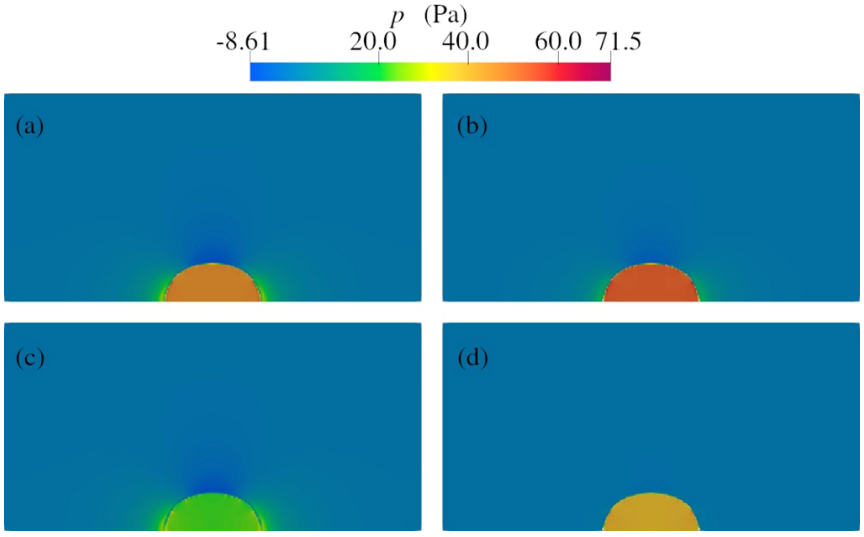

Figure 4. The pressure at the end of the simulation for the case (a) NpNp, (b) NpP, (c) PNp, (d) PP.

3.3.4. *Deformation*

The simulation time was 7.5 s. If the drop did not settle, the simulation time was extended first to 10.0 s, and, if needed, to 12.5 s.

Figure 5 shows the comparison of the obtained results and the analytically predicted results. It has already been stated in the literature that linearized asymptotic analysis was used for Eq. (28) (Bošković & Bugarski 2024). It is also stated that predictions of Eq. (29) differed from experimentally obtained deformations (Lima 2017). Hence, some deviation of the drop deformations that we obtained from analytical predictions was expected and is actually desirable.

The positive deformations from Figure 5(a) are similar to previously published results. The closeness of the obtained D_d and the analytically predicted one from Eq. (28), when Eq. (28) predicted 0.04, is similar to (López-Herrera et al. 2011). Results for D_d greater than around 0.075 are not present in (López-Herrera et al. 2011). High deviations from Eq. (28) for high Ca_e can be found in Lima and d'Ávila (2014), which are similar to the deviations presented here for high D_d. Thus, it can be concluded that the obtained results are similar to the EHD literature. On the other hand, previous results with the EMFD model presented in Bošković and Bugarski (2024)

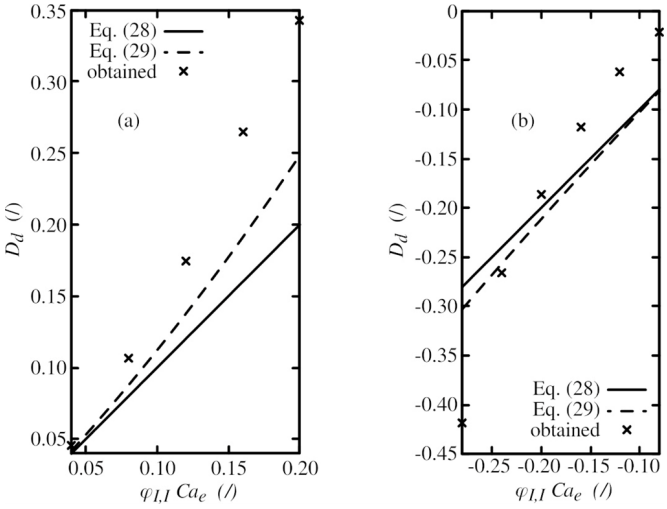

Figure 5. The obtained drop deformations – (a) positive, (b) negative.

are almost equal to the analytical predictions of Eq. (28) even for D_d equal to 0.16.

The negative deformations from Figure 5(b) cannot be as easily compared to the literature. For instance, there are no simulations with negative deformations in Singh et al. (2019). To our knowledge, negative deformations

are usually presented in the literature when R_σ is varied. Thus, Figure 5(b) can be important for future comparisons because we varied analytical D_d. Nevertheless, our result when analytical prediction was -0.20 is similar to the result from López-Herrera et al. (2011) for similar analytical prediction and R_σ.

3.4. Settling drop

An analytical equation for the drop settling velocity can be found in Behera et al. (2019); Xu and Homsy (2006):

$$\frac{|U_{d,s}|}{|U_{d,s}||_{|E|=0}} = 1 + \varphi_{s,I}\varphi_{I,I}Ca_e + \varphi_{s,II}|E_{mu}|^2 \tag{35}$$

$$\varphi_{s,I} = \frac{4}{15}\frac{3R_\mu^2 - R_\mu + 8}{(3R_\mu + 2)(R_\mu + 1)} \tag{36}$$

$$\varphi_{s,II} = -\frac{6}{5}\frac{\varepsilon_2^2}{\mu_2\sigma_2}\frac{(1-R_\varepsilon/R_\sigma)(3-R_\varepsilon+3R_\sigma)}{R_\sigma(2/R_\sigma+1)^2(3+2R_\sigma)(3R_\mu+2)(R_\mu+1)} \tag{37}$$

where subscript s denotes settling.

In these simulations, electric conductivities had 10^3 times greater values than in the simulations of a stationary drop deformation. The gravitational acceleration was equal to 9.81 m s^{-2} and was directed from the left wall to the right wall. The interfacial tension was 0.035 N m^{-1}. The mass density of Fluid 2 was 10 kg m^{-3}, while its kinematic viscosity was 0.12 m^2 s^{-1}. Other fluid properties were equal to those for stationary drop deformations.

The location of the drop center was used for determining the drop velocity. Firstly, in Paraview (with paraFoam) we isolated parts of the geometry that had α_1 equal to or greater than 0.5. After that, still in the same software, we determined the volume and the center of the remaining cells. Afterwards, we determined the volumetric drop center from the following equation:

$$x_d = \frac{1}{V_d}\sum_k x_{c,k}V_{c,k} \tag{38}$$

where subscript c denotes cell. Finally, we calculated the average drop velocity based on the starting location. The results were output every 0.025 s. After 0.5 s, we checked whether the penultimate value of the drop deformation differed by less than 0.1% from the last value. If not, we simulated 0.7 s and checked again. One simulation with the unmodified interFoam solver was done in order to obtain the ratio of the velocities that is on the left hand side of Eq. (35). The starting value for the first time step for the simulation with interFoam was 10^{-7} s. Both average velocities in the velocity ratio were for either 0.5 s or 0.7 s.

Here, the target maximum value for the Courant number and the interface Courant number was equal to 0.0005. It can be said that such a low value was not needed because of our modifications of the solver since it was needed even for the unmodified interFoam solver. The geometry height was reduced to $4r_d|_{t=0}$, and the top border was a wall to decrease computational times. The geometry width was equal to $7d_d|_{t=0}$, while the drop center was $2.5d_d|_{t=0}$ away from the left wall at the start of the simulation. The mesh had the same density as for the stationary drop.

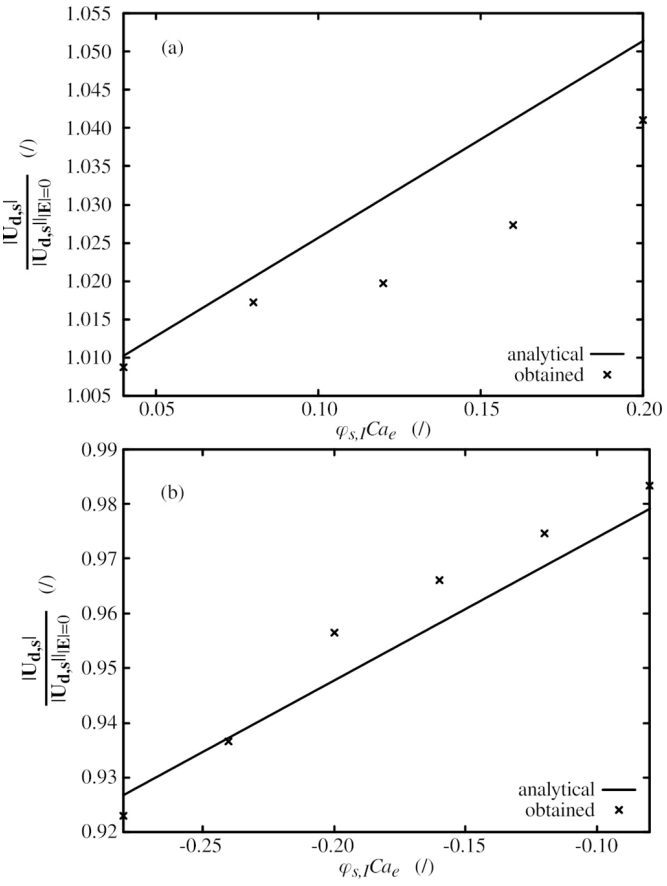

Figure 6. The ratios of settling drop velocities when D_d from Eq. (28) is (a) positive (b) negative.

Figure 6 illustrates the comparison of the analytical and the obtained results. This differs from Behera et al. (2019) because it can be seen that their results differ from the analytical predictions similar to what is usual for the stationary drop deformation. On the other hand, all laboratory experiments from Xu and Homsy (2006) do not follow analytical predictions and straight lines. Some laboratory results were above, while some were below the analytical predictions in Xu and Homsy (2006). According to Xu and Homsy (2006), this is caused by the lack

of higher order terms in Eq. (35). Thus, the results that we obtained might not be problematic and can be interesting for future comparisons. The fact that the obtained ratio is suddenly below the analytical line when D_d from Eq. (28) is -0.24 and -0.28 can be connected to the fact that in Figure 5(b) the obtained D_d is also suddenly below the analytical line. We also noticed that for these two cases (unlike the other cases with negative ratios), a pressure minimum forms along the symmetry axis inside the settling drop. It can also be said that the cases when D_d from Eq. (28) is greater than 0.08 are farther away from the analytical predictions. This can also be connected to pressure changes because the point with the highest pressure inside the drop changed its place from the front part of the drop to the back part. Nevertheless, these results suggest that the present model and its implementation predict the influence of an electric field on the settling drop. To our understanding, this is just the second scientific article in which OpenFOAM® is used for any settling drop, after Moezzi, Sajjadi, and Hejazi (2023) (in which there is no electric field).

4. CONCLUSION

A two-phase leaky dielectric model from electrohydrodynamics was successfully implemented in the computational fluid dynamics software called OpenFOAM®. The optimization of the implementation was done. Different expressions were tested for certain variables. This resulted in an optimized solver. Optimized expressions for the used software for all three electric forces are given. The expressions can be used for both more and less complex models.

A new way for calculating the electrostrictive force in systems with two fluids is given. The issue that existed in cases when one fluid was nonpolar, while the other one was polar Bošković et al. (2022a) is finally resolved. In those cases, a drop would deform, even though this was not the case when both fluids were either polar or nonpolar (Bošković et al. 2022a).

Three sets of simulations were done. The first one was one-dimensional. It was used just for optimization purposes. The second one was with a drop that is deformed by an electric field. These simulations are usual for showing the quality of a solver. Negative deformations were also simulated. The results were good when compared to the EHD literature (Lima & d'Ávila 2014; López-Herrera et al. 2011). The third set of simulations was the drop settling, where a limited number of results is available in the literature. Thus, it was difficult to analyze these results in greater detail.

These conclusions are expected to be useful for EHD and future implementations of EHD models in OpenFOAM®.

FUNDING

This work was supported by the Ministry of Science, Technological Development and Innovation of the Republic of Serbia [Contract Nos. 451-03-66/2024-03/200287, 451-03-65/2024-03/200135]; and by the Science Fund of the Republic of Serbia [The Program IDEAS MultiPromis 7751519].

DATA AVAILABILITY STATEMENT

The data that supports these findings are available from the corresponding author.

CONFLICTS OF INTEREST

The authors declare no conflict of interest.

NOMENCLATURE

Roman symbols

Ca → Capillary number (/)
Co → Courant number (/)
D → deformation (/)
d → diameter (m)
$\boldsymbol{E}$ → electric field strength ($V \cdot m^{-1}$)
$\boldsymbol{F}$ → force (N)
f → function (/)
$\boldsymbol{g}$ → gravitational acceleration ($m \cdot s^{-2}$)
$\boldsymbol{I}$ → identity tensor (/)
l → length (m)
$\boldsymbol{n}$ → unit normal vector (/)
p → pressure (Pa)
R → ratio of property in subscript of Fluid 1 and Fluid 2 (/)
R → reconstruction function
$\boldsymbol{S}$ → surface area vector (m^2)
T → temperature (K)
t → time (s)
$\boldsymbol{T}_e$ → Maxwell stress tensor ($N \cdot m^{-2}$)
$\boldsymbol{U}$ → velocity ($m \cdot s^{-1}$)
x → axis (m)
z → variable

Greek symbols

ε → electric permittivity (F·m^{-1})
α → volume fraction (/)
μ → viscosity (Pa·s)
ρ → mass density (kg·m^{-3})
ρ_e → electrical charge density (C·m^{-3})
σ → electric conductivity (S·m^{-1})
ϕ → electric potential (V)
φ → function

Subscripts

0 → vacuum
C → Coulombic
c → cell
d → drop
die → dielectric
e → electric
$elec$ → electrolysis
f → cell face
j → fluid j ($j = 1, 2$)
l → left
mix → macroscopically uniform
n → direction normal to E
q → other electric
p → direction parallel to E
r → right
s → settling
st → surface tension
w → between walls

Abbreviations

CFD → computational fluid dynamics
EHD → electrohydrodynamics
EMFD → electromagnetic fluid dynamics
FVM → Finite-Volume Method
VoF → Volume of Fluid

REFERENCES

Behera, N., Mandal, S., & Chakraborty, S. (2019). Electrohydrodynamic settling of drop in uniform electric field: Beyond Stokes flow regime. *Journal of Fluid Mechanics*, *881*, 498–523. https://doi.org/10.1017/jfm.2019.744

Bošković, S., & Bugarski, B. (2018). Review of electrospray observations and theory. *Journal of Engineering & Processing Management*, *10*(2), 41–53. https://doi.org/10.7251/jepm181002041b

Bošković, S., & Bugarski, B. (2024). Two-phase electromagneto-fluid dynamics model and its computational fluid dynamics implementation. *Physics of Fluids*, *36*(2). https://doi.org/10.1063/5.0190651

Bošković, S., Karač, A., Vrhovac, S., Belić, A., & Bugarski, B. (2022a). Implementation of the electrohydrodynamics' perfect dielectric model in OpenFOAM®. *Journal of Engineering & Processing Management*, *14*(2). https://doi.org/10.7251/JEPM2202066b

Bošković, S., Karač, A., Vrhovac, S., Belić, A., & Bugarski, B. (2022b). Investigation of electrohydrodynamic calculations. *Hemijska industrija*, *76*(2), 65–74. https://doi.org/10.2298/HEMIND211110010B

Bugarski, B., Li, Q., Goosen, M., Poncelet, D., Neufeld, R., & Vunjak, G. (1994). Electrostatic droplet generation: Mechanism of polymer droplet formation. *AIChE Journal*, *40*(6), 1026–1031. https://doi.org/10.1002/aic.690400613

Bugarski, B., Smith, J., Wu, J., & Goosen, M. (1993). Methods for animal cell immobilization using electrostatic droplet generation. *Biotechnology Techniques*, *7*(9), 677–682. https://doi.org/10.1007/BF00151869

Dastourani, H., Jahannama, M. R., & Eslami-Majd, A. (2018). A physical insight into electrospray process in cone-jet mode: Role of operating parameters. *International Journal of Heat and Fluid Flow*, *70*, 315–335. https://doi.org/10.1016/j.ijheatfluidflow.2018.02.012

He, T., & Jokerst, J. (2020). Structured micro/nano materials synthesized via electrospray: A review. *Biomaterials Science*, *8*(20), 5555–5573. https://doi.org/10.1039/d0bm01313g

Huh, H., & Wirz, R. E. (2022). Simulation of electrospray emission processes for low to moderate conductivity liquids. *Physics of Fluids*, *34*(11), 112017. https://doi.org/10.1063/5.0120737

Ionescu, A. (Ed.). (2018). *Computational fluid dynamics: Basic instruments and applications in science*. Rijeka, Croatia: InTech. https://doi.org/10.5772/intechopen.68688

Kunti, G., Bhattacharya, A., & Chakraborty, S. (2017). A scaling analysis for electrohydrodynamic convection with variable thermophysical and electrical properties. *International Journal of Heat and Mass Transfer*, *109*, 215–222. https://doi.org/10.1016/j.ijheatmasstransfer.2017.01.104

Lastow, O., & Balachandran, W. (2006). Numerical simulation of electrohydrodynamic (EHD) atomization. *Journal of Electrostatics*, *64*(12), 850–859. https://doi.org/10.1016/j.elstat.2006.02.006

Leary, T., Yeganeh, M., & Maldarelli, C. (2020). Microfluidic study of the electrocoalescence of aqueous droplets in crude oil. *ACS Omega*, *5*(13), 7348–7360. https://doi.org/10.1021/acsomega.9b04259

Lebaigue, O. (2010). Two-phase microflows. In S. Colin (Ed.), *Two-phase microflows*. London, UK and Hoboken, NJ, USA: ISTE Ltd and John Wiley & Sons, Inc.

Lima, N. (2017). *Numerical studies in electrohydrodynamics* (Unpublished doctoral dissertation). School of Mechanical Engineering of the University of Campinas.

Lima, N., & d'Ávila, M. (2014). Numerical simulation of electrohydrodynamic flows of Newtonian and viscoelastic droplets. *Journal of Non-Newtonian Fluid Mechanics*, *213*, 1–14. https://doi.org/10.1016/j.jnnfm.2014.08.016

López-Herrera, J., Popinet, S., & Herrada, M. (2011). A charge-conservative approach for simulating electrohydrodynamic two-phase flows using volume-of-fluid. *Journal of Computational Physics*, *230*(5), 1939–1955. https://doi.org/10.1016/j.jcp.2010.11.042

Maliska, C. R. (2023). *Fundamentals of computational fluid dynamics: The finite volume method*. Cham, Switzerland: Springer Nature Switzerland AG. https://doi.org/10.1007/978-3-031-18235-8

Manojlovic, V., Djonlagic, J., Obradovic, B., Nedovic, V., & Bugarski, B. (2006). Immobilization of cells by electrostatic droplet generation: A model system for potential application in medicine. *International Journal of Nanomedicine*, *1*(2), 163–171. https://doi.org/10.2147/nano.2006.1.2.163

Moezzi, M., Sajjadi, M., & Hejazi, S. H. (2023). Thermally driven Marangoni effects on the spreading dynamics of droplets. *International Journal of Multiphase Flow*, *159*, 104335. https://doi.org/10.1016/j.ijmultiphaseflow.2022.104335

Munoz, C. N. (2014). *Computational modelling of electrohydrodynamic atomization* (Unpublished master's thesis). The University of Manchester, Manchester, UK.

Poncelet, D., Babak, V., Neufeld, R., Goosen, M., & Burgarski, B. (1999). Theory of electrostatic dispersion of polymer solutions in the production of microgel beads containing biocatalyst. *Advances in Colloid and Interface Science*, *79*(2-3), 213–228. https://doi.org/10.1016/S0001-8686(97)00037-7

Poncelet, D., Bugarski, B., Amsden, B., Zhu, J., Neufeld, R., & Goosen, M. (1994). A Parallel plate electrostatic droplet generator: Parameters affecting microbead size. *Applied Microbiology and Biotechnology*, *42*(2–3), 251–255. https://doi.org/10.1007/BF00902725

Reddy, M., & Esmaeeli, A. (2009). The EHD-driven fluid flow and deformation of a liquid jet by a transverse electric field. *International Journal of Multiphase Flow*, *35*(11), 1051–1065. https://doi.org/10.1016/j.ijmultiphaseflow.2009.06.008

Shneider, M., & Pekker, M. (2013). Dielectric fluid in inhomogeneous pulsed electric field. *Physical Review E*, *87*(4), 043004. https://doi.org/10.1103/PhysRevE.87.043004

Singh, R., Bahga, S., & Gupta, A. (2019). Electrohydrodynamics in leaky dielectric fluids using lattice Boltzmann method. *European Journal of Mechanics - B/Fluids*, *74*, 167–179. https://doi.org/10.1016/j.euromechflu.2018.11.011

Supeene, G., Koch, C., & Bhattacharjee, S. (2008). Deformation of a droplet in an electric field: Nonlinear transient response in perfect and leaky dielectric media. *Journal of Colloid and Interface Science*, *318*(2), 463–476. https://doi.org/10.1016/j.jcis.2007.10.022

Taylor, J. (2011). *Optical binding phenomena: Observations and mechanisms*. Germany: Springer-Verlag Berlin Heidelberg. https://doi.org/10.1007/978-3-642-21195-9

Thirumalaisamy, R., Natarajan, G., & Dalal, A. (2018). Towards an improved conservative approach for simulating electrohydrodynamic two-phase flows using volume-of-fluid. *Journal of Computational Physics*, *367*, 391–398. https://doi.org/10.1016/j.jcp.2018.04.024

Torchigin, V., & Torchigin, A. (2013). Interrelation between various types of optically induced forces. *Optics Communications*, *301–302*, 147–151. https://doi.org/10.1016/j.optcom.2013.03.041

Vaseashta, A., & Bölgen, N. (Eds.). (2022). *Electrospun nanofibers: Principles, technology and applications*. Cham, Switzerland: Springer Nature Switzerland AG. https://doi.org/10.1007/978-3-030-99958-2

Xu, X., & Homsy, G. (2006). The settling velocity and shape distortion of drops in a uniform electric field. *Journal of Fluid Mechanics*, *564*, 395–414. https://doi.org/10.1017/S0022112006001480